Supporting Information

Aqueous-Organic Hybrid Electrolyte Stabilizing Zinc Metal Anodes

Liwen Hu,[a] Yaping Song,[a] Xinyue Li,[a] Keming Hu,[c] and Yang Song,*[ab]

a. College of Materials Science and Engineering, Chongqing University, Chongqing 400044, PR China.

b. National Innovation Center for Industry-Education Integration of Energy Storage Technology, Chongqing University, Chongqing, 400044, China.

c. Carlson school of management, University of Minnesota, twin cities, Minnesota, 55455, USA.

Corresponding author Email: ysong0423@cqu.edu.cn.

Experimental Section

Electrolyte synthesis. Hydrated zinc tetrafuoroborate ($Zn(BF_4)_2$ xH_2O, chemically pure), and DMF (analytical reagents, ⩾99%) were purchased from Aladdin. Deionized water was used as the solvent to prepare the aqueous electrolytes. A series of DMF/H_2O solvents were prepared by regulating the volume ratios (V_{DMF}: V_{H2O}) of 10: 1, 9: 1,8: 1, 4:1. The mixture was subsequently sealed in a glass container and agitated for a duration of four hours, resulting in a transparent and uniform solution. Electrolytes with varying $Zn(BF_4)_2$ concentrations-0.23M, 0.44 M, 0.81 M, 1.22 M, 1.65 M, and 2.53 M-were formulated by adding incremental amounts of $Zn(BF_4)_2$ xH_2O to the DMF/H_2O base electrolyte with the volume ratios of 8: 1. For instance, the 0.44 M electrolyte was produced by incorporating 3.034 g of $Zn(BF_4)_2$ xH_2O into 18 ml of DMF/H_2O (V_{DMF}: V_{H2O}=8: 1), followed by stirring for four hours, resulting in a uniform and transparent solution.

Characterization. The morphologies of the as-prepared samples were studied with Scanning Electron Microscopy (SEM, 5 kV, Quattro S). X-ray diffraction (XRD) tests were performed on a Rigaku SmartLab diffractometer using Cu Ka radiation (λ = 1.54178Å). Fourier-transform infrared spectroscopy (FTIR) was performed on a Bruker Alpha-P instrument with attenuated total reflection (ATR) technology in the frequency range of 400-4000 cm^{-1}. TGA was performed on a Mettler Toledo TGA-DSC analyser under a nitrogen atmosphere. The valence state and chemical composition were analyzed by X-ray photoelectron spectroscopy (XPS, Thermo Kalpha), with binding energies referenced to the C 1s peak at 284.8 eV. The Raman spectra were collected using a LabRAM HR Evolution spectrometer with a 532 nm laser.

Electrochemical measurements. We performed electrochemical evaluations on both symmetric and half-cell configurations using CR2032 coin cells, separated by a Whatman GF/A glass fiber and immersed in various concentrations of $Zn(BF_4)_2$ DMF/H_2O electrolyte or aqueous electrolytes. The electrochemical tests, including LSV and Tafel were conducted at 30 ℃ using either Chenhua CHI-660E electrochemical workstation or a Neware battery testing system. LSV measurements utilized a three-electrode setup, operating at a scan rate of 10 mV s^{-1}. For full cells, we used an electrolyte composed of either with/without DMF mixed with 0.44 M $Zn(BF_4)_2$ xH_2O.

DFT calculations: *DFT calculations***:** Density functional theory (DFT) was used to calculate the binding energy and visualize the electrostatic potential maps, which was implemented by the Dmol3 program packaging in Materials Studio**.** In our work, BLYP with hybrid density functional method, had been adopted to optimize the geometries in these structures. The Binding energies were obtained by $E_{b-e} = E_{A-B} - (E_A+E_B)$, where E_{A-B}, E_A and E_B are the energies of the A-B species binding, the energy of the A species and the energy of the B species, respectively.

Molecular dynamic simulations related details: Molecular dynamic simulations were performed using the Forcite module in Materials Studio. The force field and charge were set for each molecule, and the force field type was set to COMPASSII. According to the molecular ratios in the experiment, the molecules were mixed in a cubic box. As shown in the **Table S1**. In the process of molecular dynamic simulation, the 5000-step steepest descent method and 5000-step conjugate gradient method were used to avoid unreasonable contact of the system. A NVT ensemble was carried out at 298 K for 1 ns. The NPT ensemble was used at 298 K for 50 ns, the pressure was maintained at 1 atm, and the integral step is 1 fs. The final 30 ns production trajectories were used to calculate radial distribution functions (RDF) and coordination structure counting analyses.

Physical field simulation modeling and calculation related details*:* The electrochemical reaction kinetic of zinc species at the anode interface in zinc metal batteries were modeled using COMSOL Multiphysics 6.2, a software for multi-physics field coupling simulations. The dimensions of the two-dimensional model, which encompassed concentration, electric field distribution, and zinc deposition analysis, were set at 45×25 μm. In this model, the relevant physical property parameters are detailed in **Table S2**.

Results and Discussion

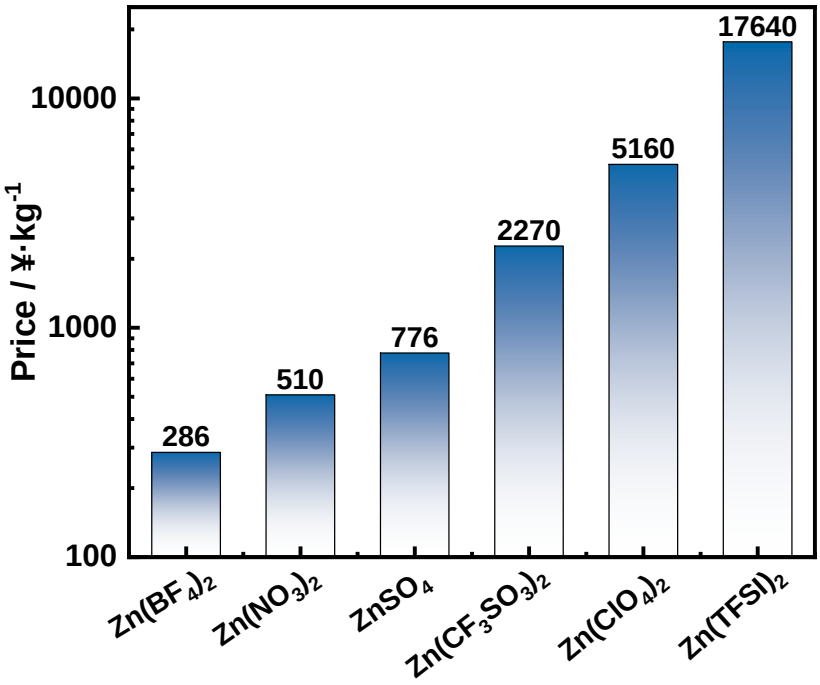

Fig. S1 Price of various Zn salts

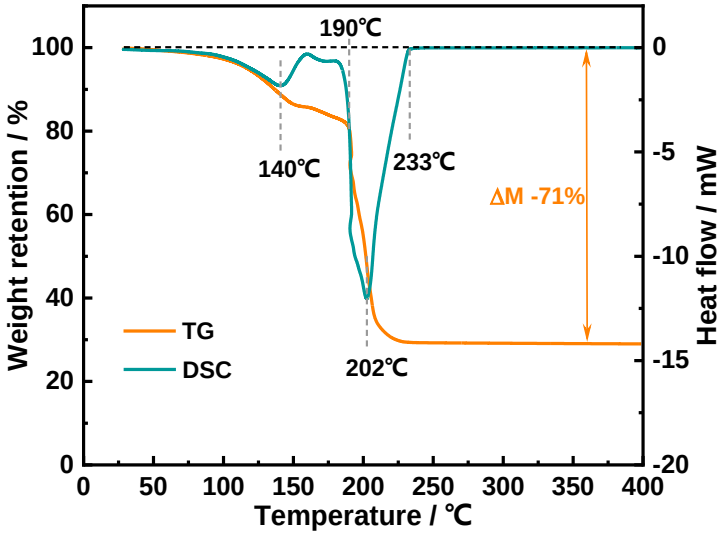

Fig. S2 TGA curve of the hydrated $Zn(BF_4)_2$ salt.

In the TGA curve, the first weight loss is attributed to partial release of water below 120 ℃. The second weight loss at 160~200 ℃ is due to both the release of more hydrated water and the decomposition of $Zn(BF_4)_2$. As shown in the XRD result, the residual solid after TGA is entirely ZnF_2. According to the weight of ZnF_2, the contents of $Zn(BF_4)_2$ and water in the hydrated salt can be calculated based on the mass conservation law using the equation of $x = n_3/n_2 = (m_3/M_3)/(m_2/M_2) = [(a - M_2b/M_1)/M_3]/(b/M_1) = (M_1a - M_2b)/(M_3b)$, where x is the molar ratio of water to $Zn(BF_4)_2$ in the hydrated $Zn(BF_4)_2$ salt; n_2 and n_3 are the amount of $Zn(BF_4)_2$ and H_2O, respectively; m_2 and m_3 are the mass of $Zn(BF_4)_2$ and H_2O, respectively; M_1, M_2 and M_3 are the molar mass of ZnF_2, $Zn(BF_4)_2$ and H_2O, respectively; a is the weight of the pristine hydrated $Zn(BF_4)_2$ salt; b is the weight of the residual ZnF_2 after TGA test. Accordingly, the x value in the hydrated $Zn(BF_4)_2$ salt is 6.5.

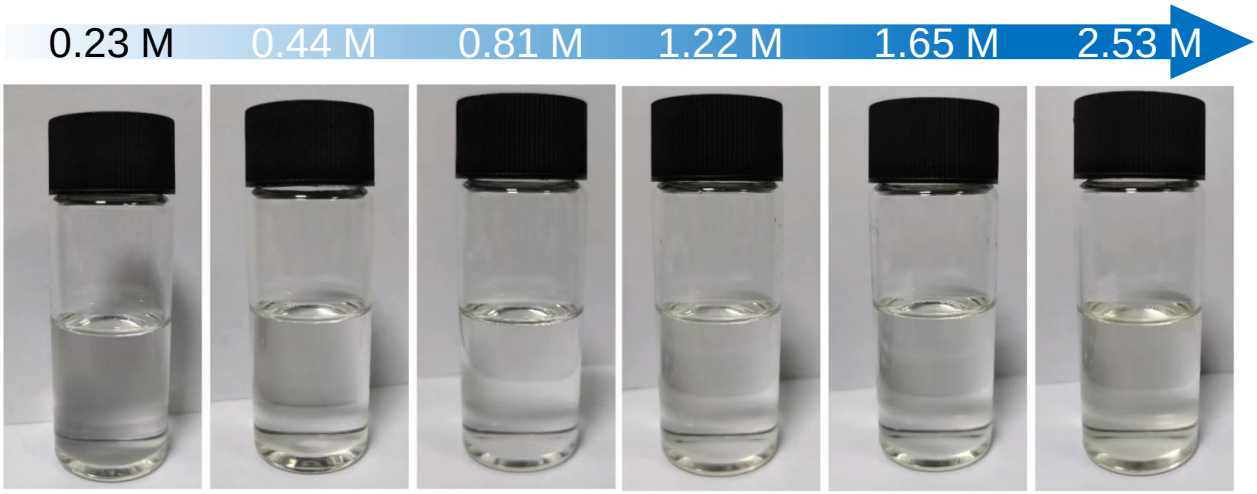

Fig. S3 The optical photographs of different $C_{Zn(BF4)2}$ electrolyte at 30℃

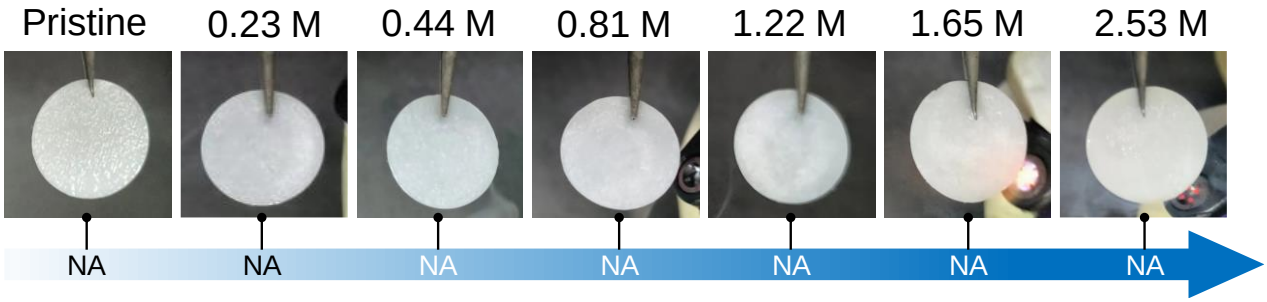

Fig. S4 Ignition tests of glass fiber separators using $C_{Zn(BF4)2}$ electrolyte

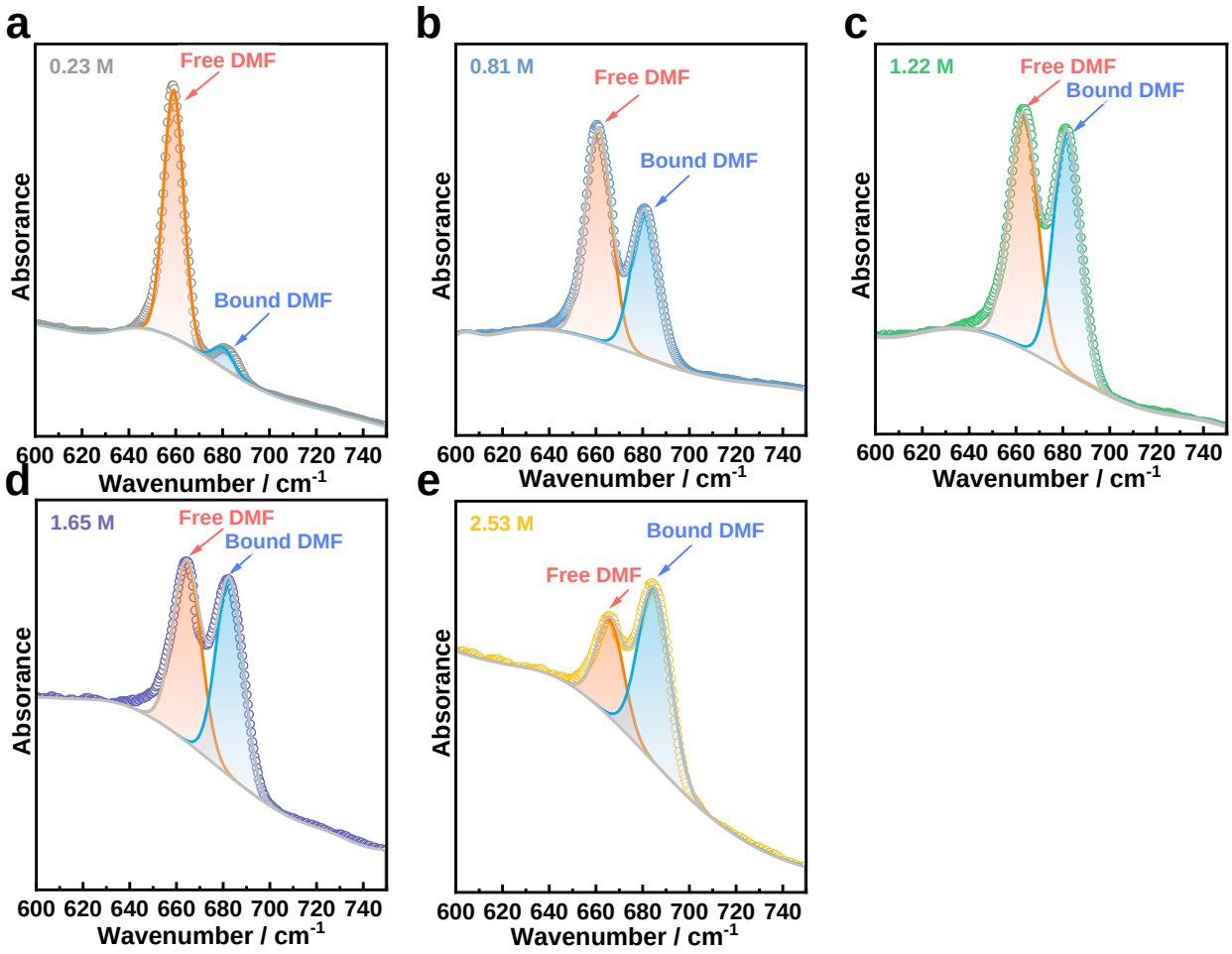

Fig. S5 The fitted peaks of ATR-FTIR spectra of various $C_{Zn(BF4)2}$ electrolyte: a) 0.23 M; b) 0.81 M; c) 1.22 M; d) 1.65 M; e) 2.53 M;

Table S1 The electrolyte with/without DMF model systems simulated in this work

System	Zn^{2+}	BF_4^-	H_2O	DMF
DMF/H_2O 8: 1	6	12	117	146
DMF/H_2O 4: 1	6	12	192	143
DMF/H_2O 2: 1	6	12	294	119
AEs	6	12	804	\

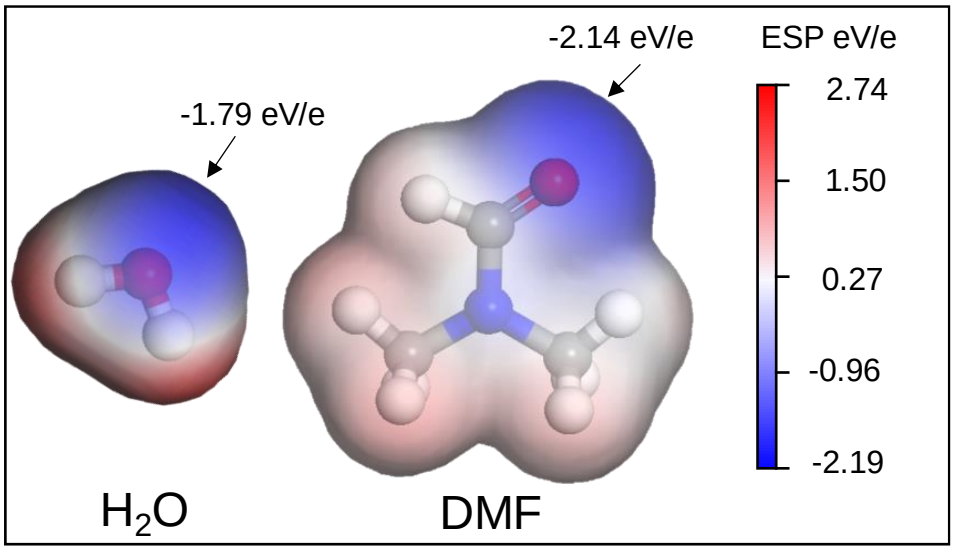

Fig. S6 ESP distribution of H_2O and DMF, Red and blue colors of the scale bar reflect higher and lower potential, respectively

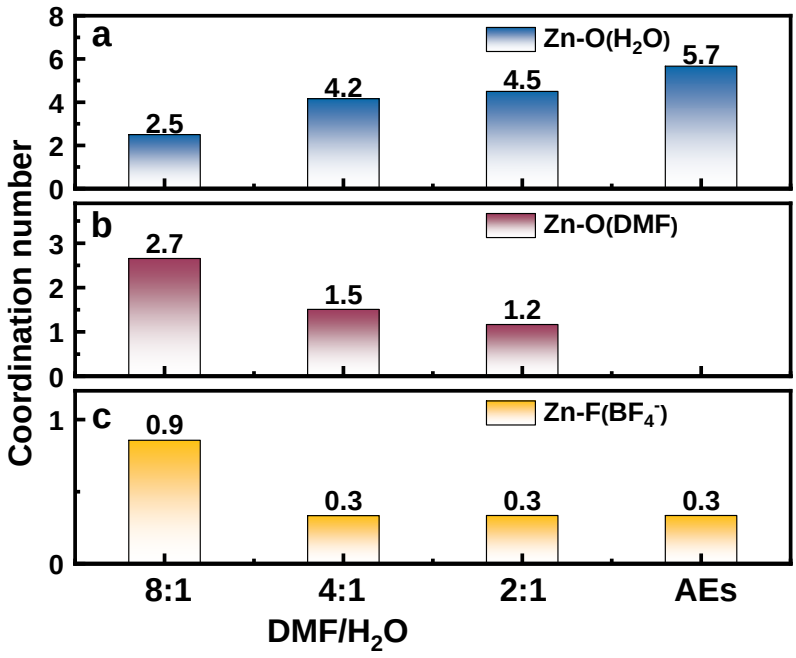

Fig. S7 The CN of a) Zn^{2+}-H_2O; b) Zn^{2+}-DMF; c) Zn^{2+}-BF_4^- collected from MD simulations with various molar ratio of DMF to H_2O electrolytes

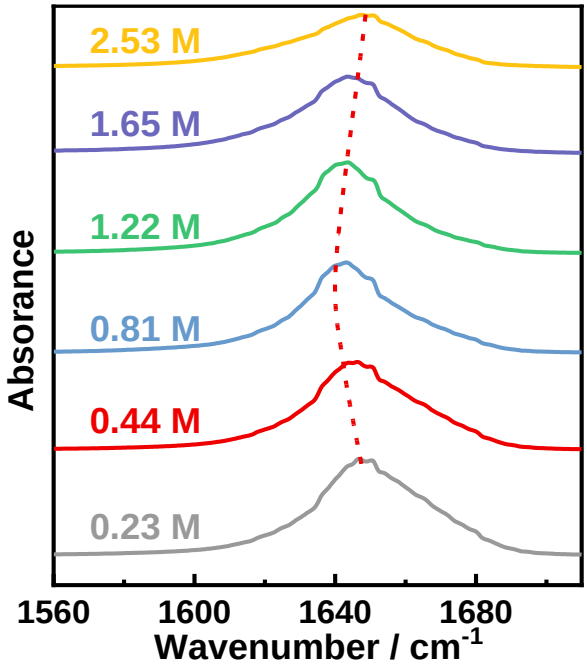

Fig. S8 ATR-FTIR spectra from 1560 ~ 1700 cm^{-1} of various $C_{Zn(BF4)2}$

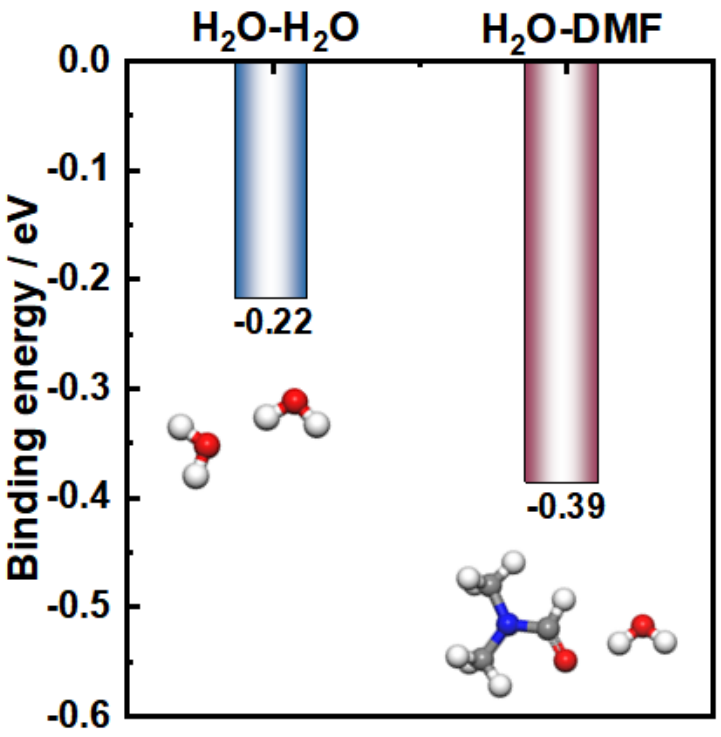

Fig. S9 The calculated binding energy of H_2O-H_2O, H_2O-DMF

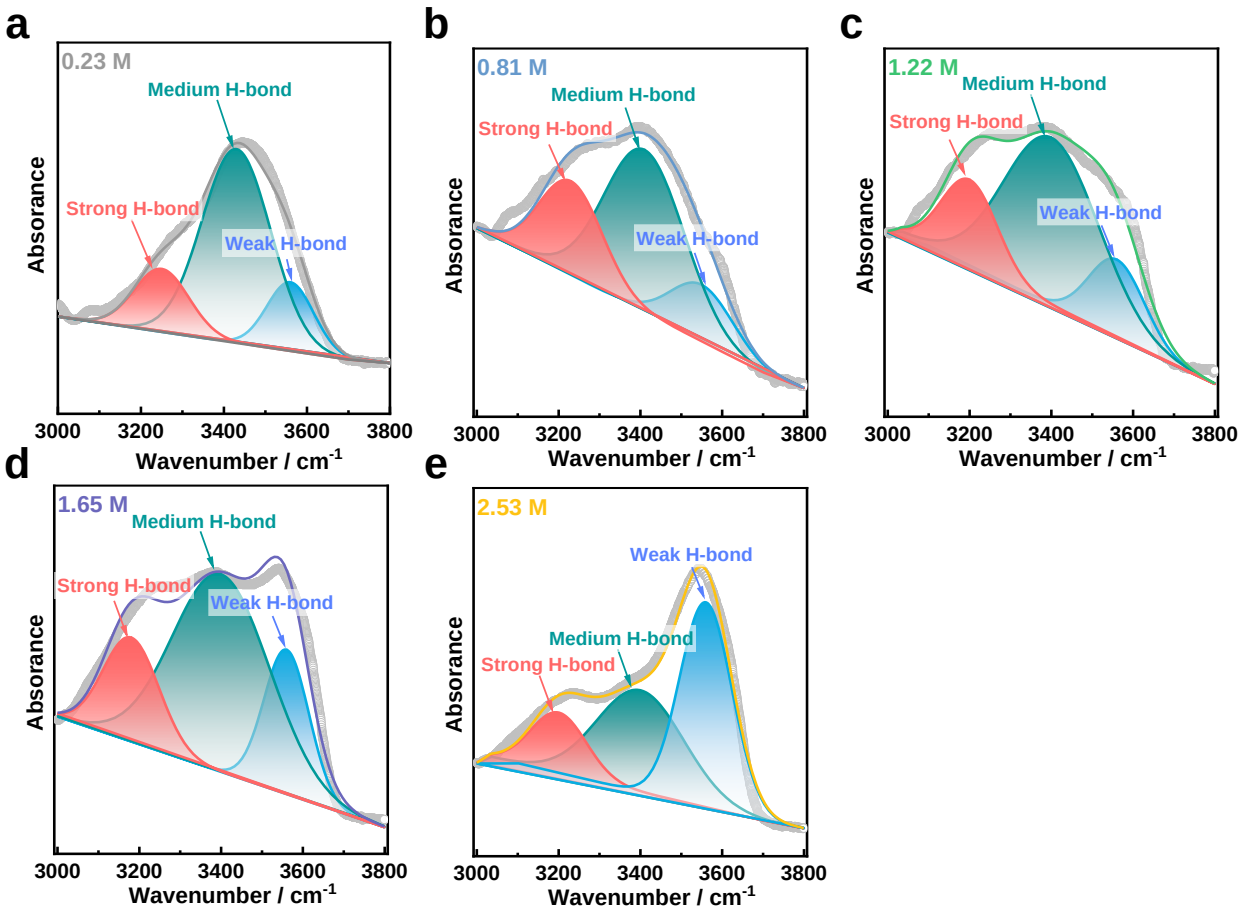

Fig. S10 The fitted peaks of ATR-FTIR spectra of various $C_{Zn(BF4)2}$ electrolyte: a) 0.23 M; b) 0.81 M; c) 1.22 M; d) 1.65 M; e) 2.53 M;

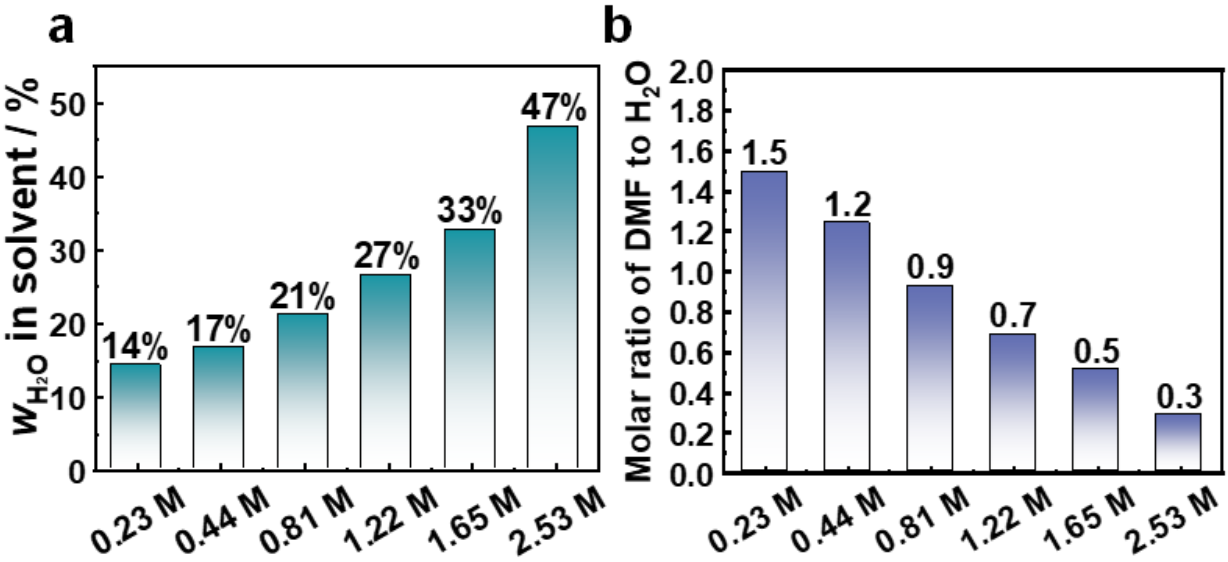

Fig. S11 a) Mass percent of water in solvent with various $C_{Zn(BF_4)_2;}$ b) Molar ratio of DMF to H_2O with various $C_{Zn(BF_4)_2}$

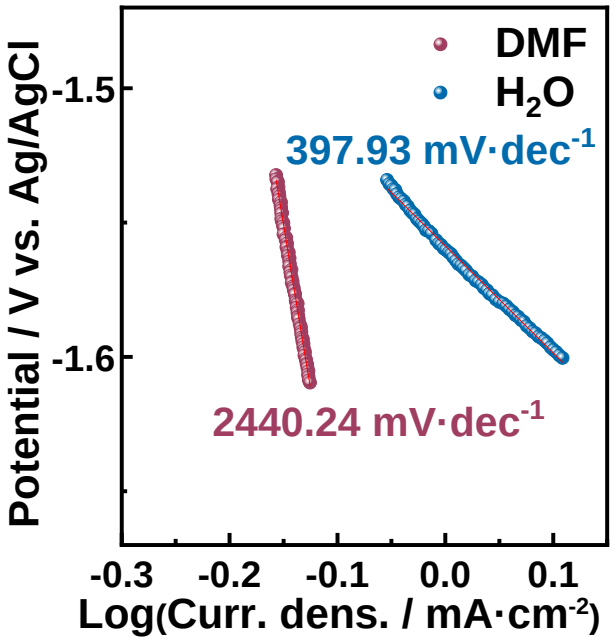

Fig. S12 Corresponding Tafel slope curves with/without DMF

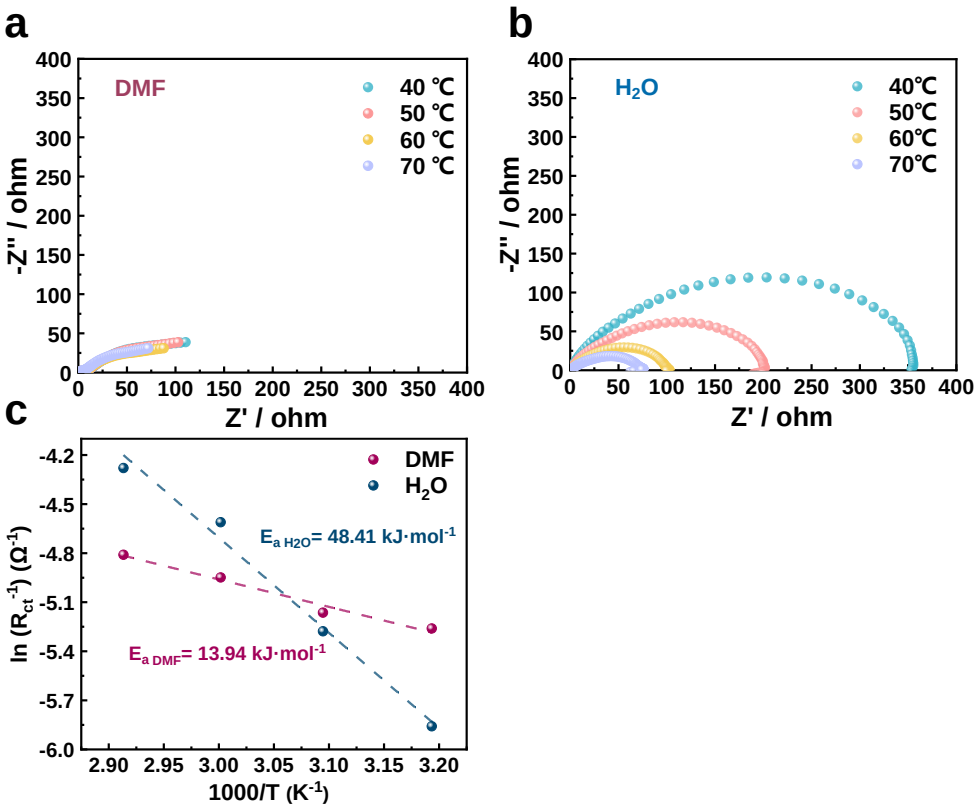

Fig. S13 a, b) Nyquist plots of Zn||Zn symmetric cells with/without DMF at different temperatures and c) the desolvation activation energy that was calculated according to the Arrhenius equation.

The de-solvation energy of Zn^{2+} ions was determined through temperature-dependent electrochemical impedance spectroscopy (EIS) measurements. Based on the Arrhenius equation ($1/Rct = A \exp(-Ea/RT)$), where Rct represents charge transfer resistance derived from the semicircle in Nyquist plots (Figs.S13a and b), and A, T, R, and Ea denote the pre-exponential factor, absolute temperature, ideal gas constant, and activation energy, respectively, the activation energies (E_a) for Zn||Zn symmetric cells were calculated as 13.94 kJ mol^{-1} in 0.44 M DMF/H_2O electrolyte versus 48.41 kJ mol^{-1} in aqueous electrolyte (Fig. S13c). The reduced E_a value (Δ34.47 kJ mol^{-1}) confirms that ZnF_2-enriched solid electrolyte interphase (SEI) formation significantly enhances interfacial redox kinetics

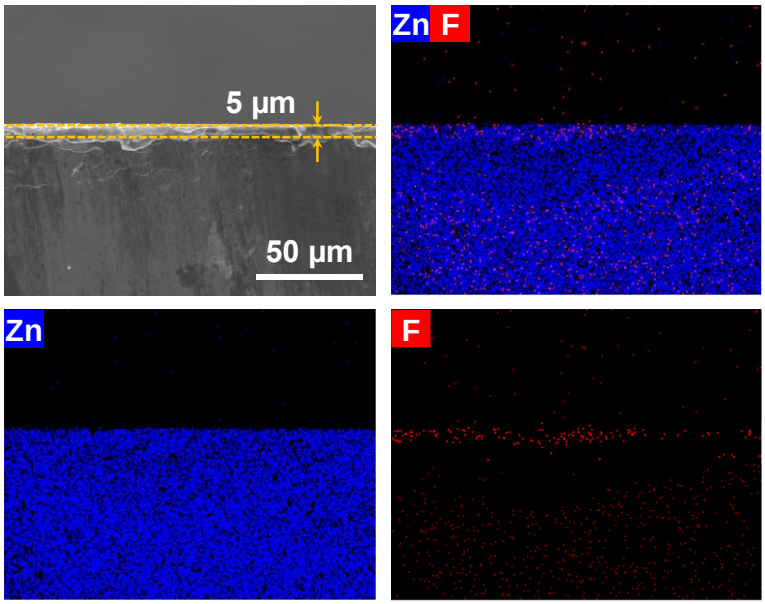

Fig. S14 SEM and EDS mapping of Zn anode after immersion in $Zn(BF_4)_2$-DMF

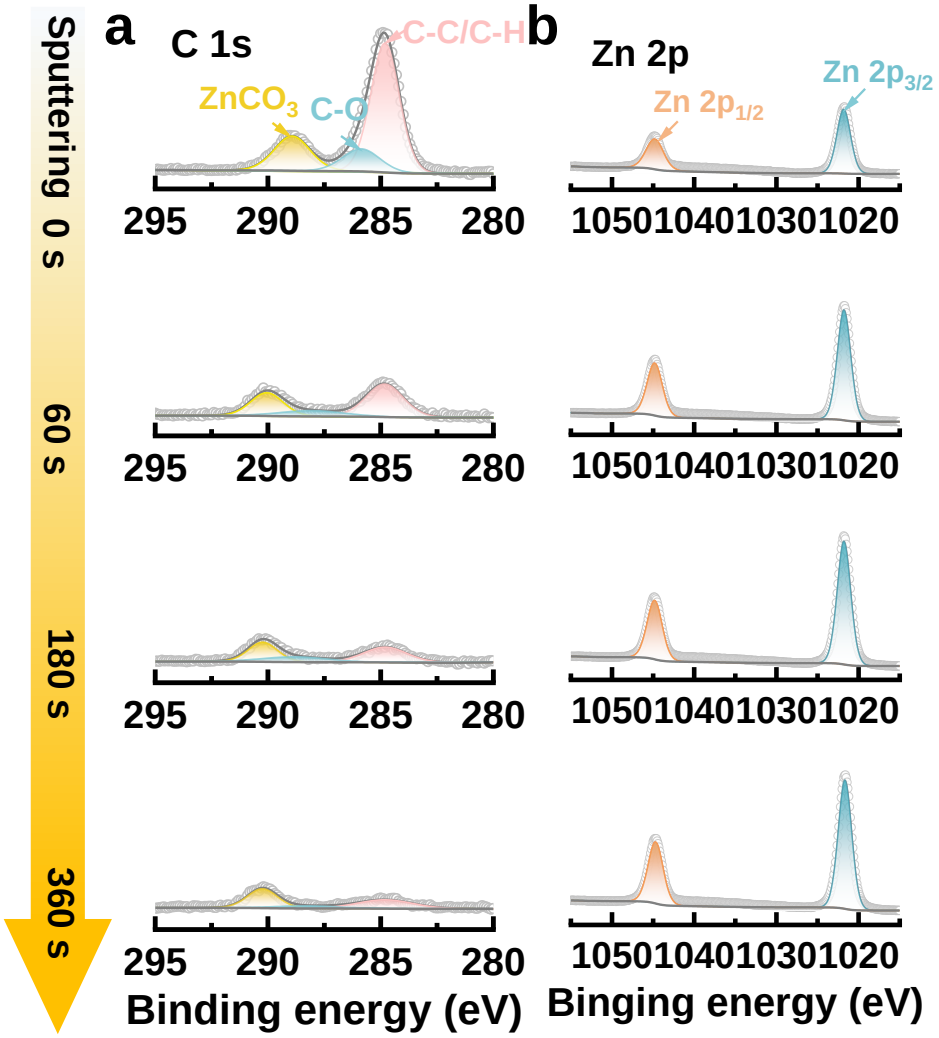

Fig. S15 Depth-profiling XPS spectra of a) C 1 s, b) Zn 2p of the Zn anode immersion with $Zn(BF_4)_2$-DMF

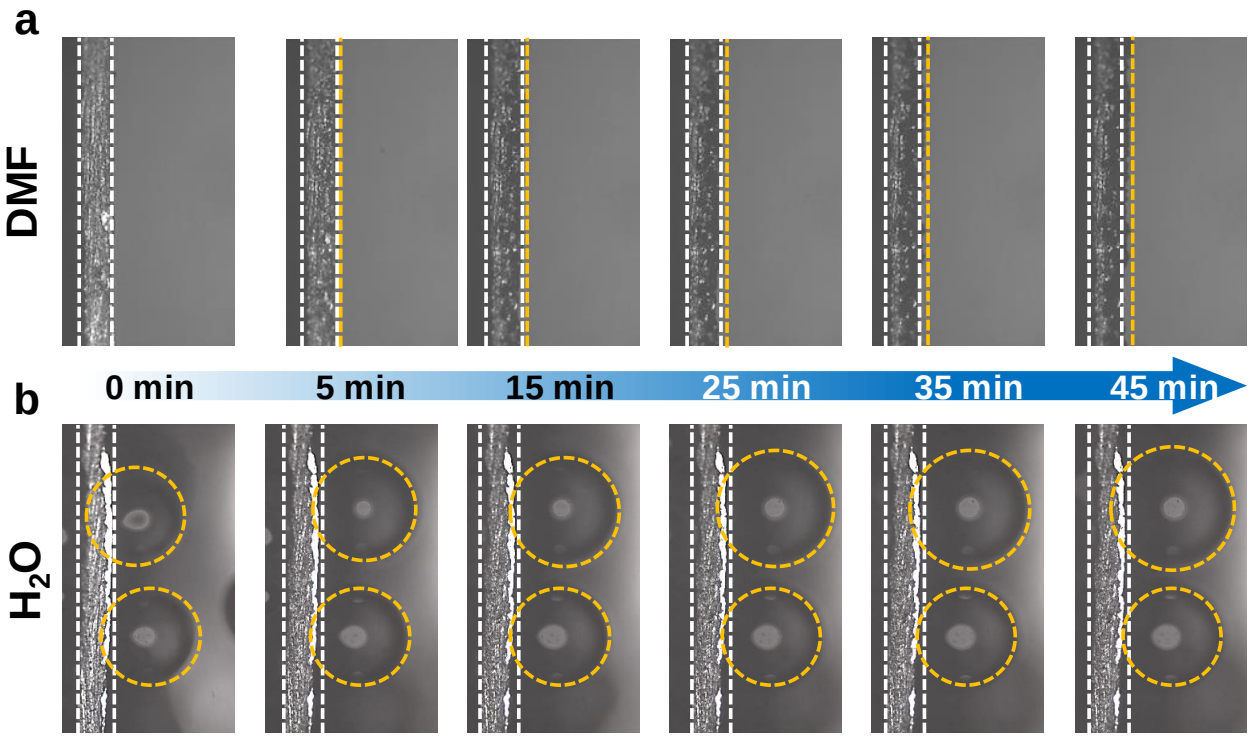

Fig. S16 In situ observations of zinc deposition in **a)** DMF-based electrolyte and **b)** AEs.

Table S2 Physicochemical properties with/without DMF of 0.44 M $Zn(BF_4)_2$ electrolytes.

System	$C_{Zn(BF4)2}$ / $mol \cdot m^{-3}$	E^0 / mV	j^0 / Am^{-2}	Ionic conductivity / $S \cdot m^{-1}$	Diffusion coefficient / $m^2 \cdot s^{-1}$
AEs	440	-56	21.78	10.21	5.73E-12
DMF-based	440	-7	65.46	2.120	8.60E-12

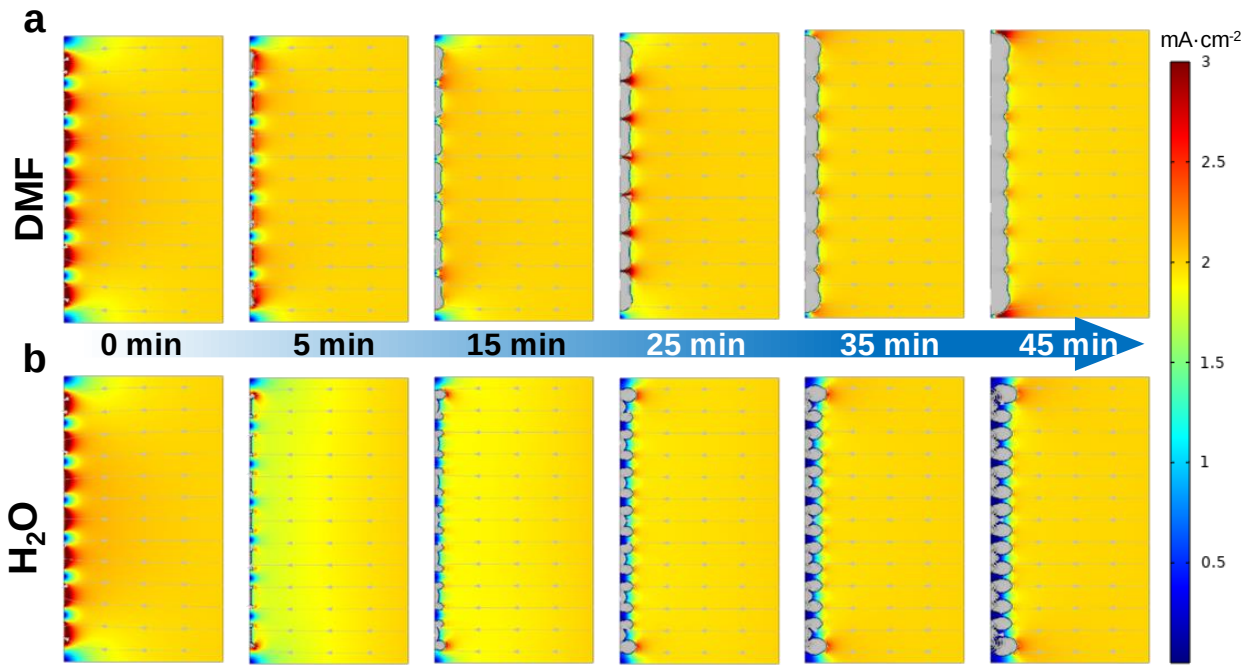

Fig. S17 The corresponding simulated morphology with distribution of current density with **a)** DMF-based electrolyte; **b)** with AEs

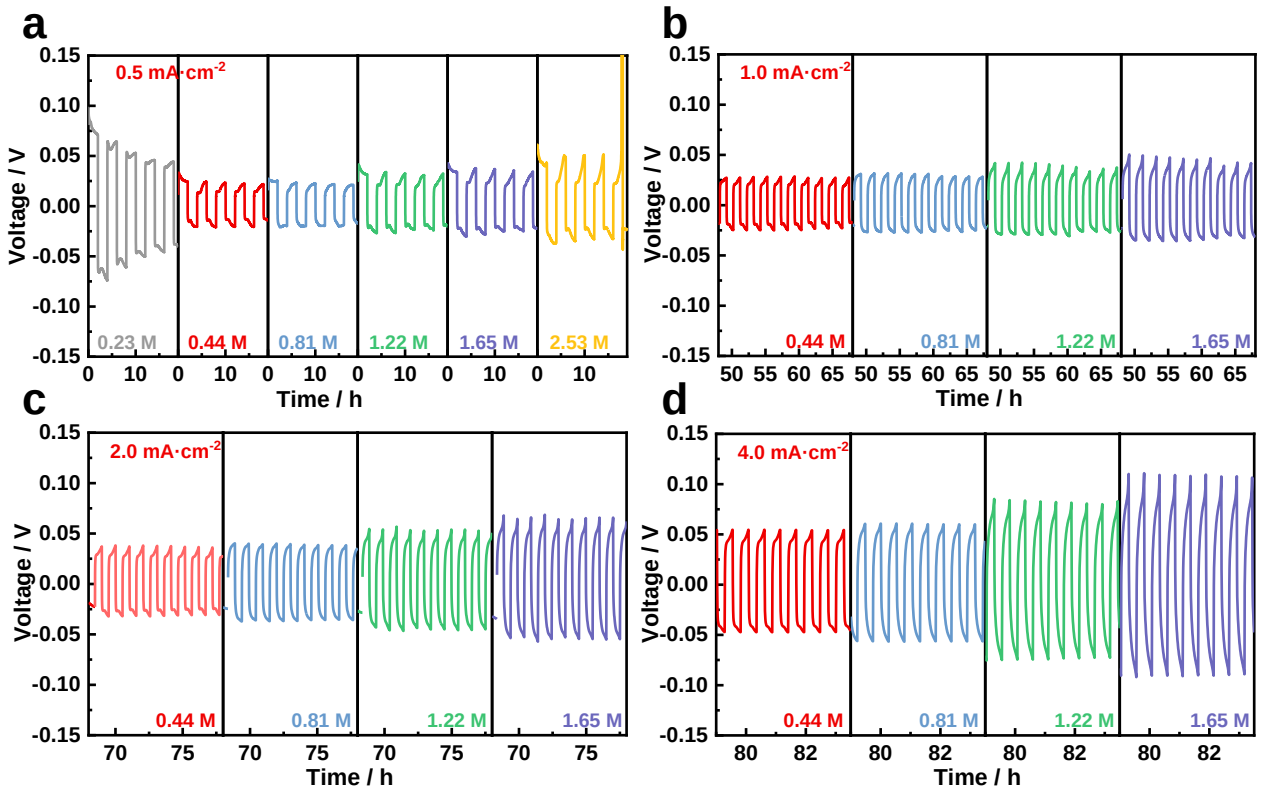

Fig. S18 Voltage-capacity curves for different $C_{Zn(BF4)2}$ electrolytes for different current density, a) 0.5 mA cm^{-2}; b) 1.0 mA cm^{-2}; c) 2.0 mA cm^{-2}; d) 4.0 mA cm^{-2};

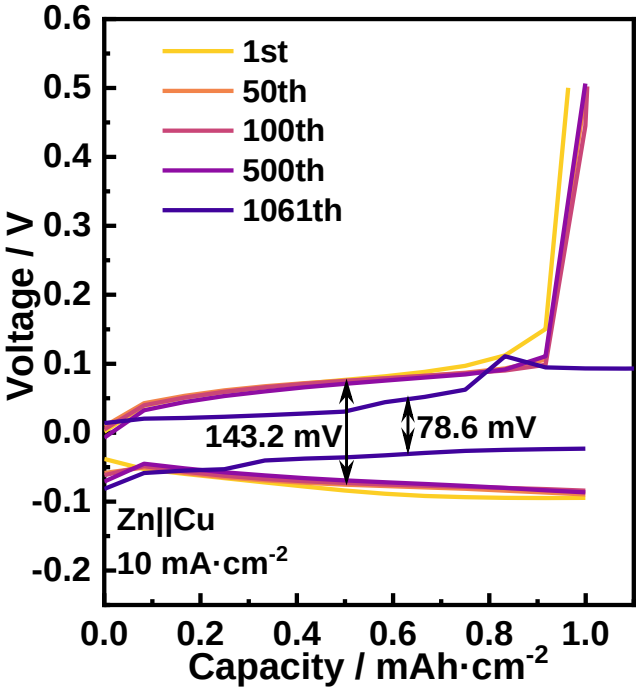

Fig. S19 The voltage profiles without DMF

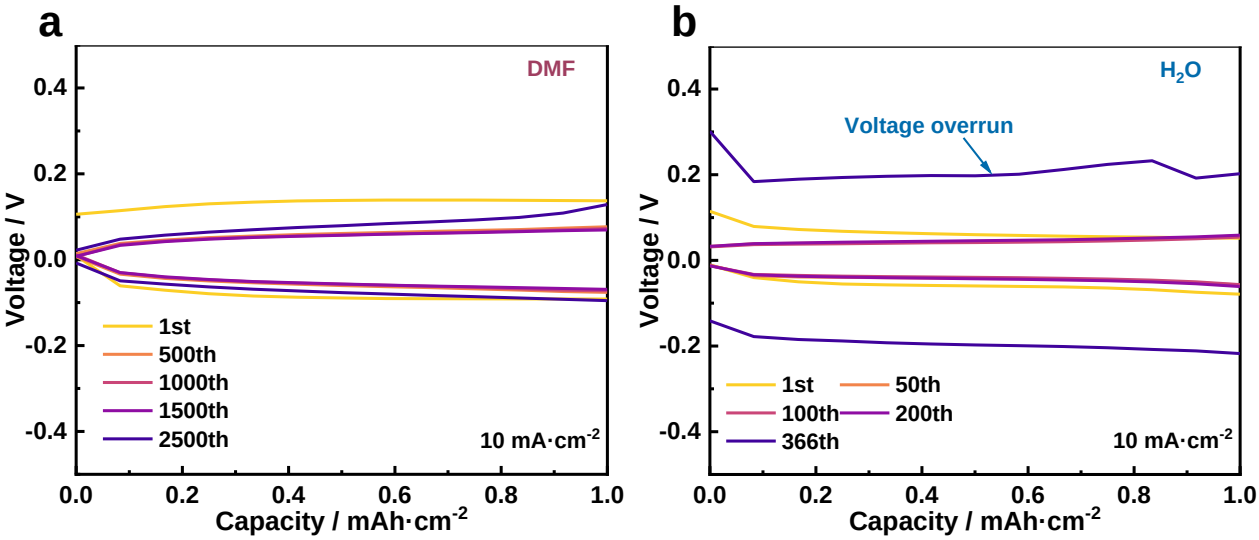

Fig. S20 Voltage-capacity curves for a) DMF and b) without DMF electrolytes at 10 mA cm^{-2} for different cycles;